Advanced Power Synchronization Control of Modular Multilevel Converter in Stiff Grid

Liu, Wentao; Teodorescu, Remus; Kerekes, Tamas; Dragicevic, Tomislav

Published in:
Proceedings of IECON 2022 – 48th Annual Conference of the IEEE Industrial Electronics Society

Link to article, DOI:
10.1109/IECON49645.2022.9968849

Publication date:
2022

Document Version
Peer reviewed version

Advanced Power Synchronization Control of Modular Multilevel Converter in Stiff Grid

Wentao Liu
Department of Energy
Aalborg University
Aalborg, Denmark
wliu@energy.aau.dk

Remus Teodorescu
Department of Energy
Aalborg University
Aalborg, Denmark
ret@energy.aau.dk

Tamas Kerekes
Department of Energy
Aalborg University
Aalborg, Denmark
tak@energy.aau.dk

Tomislav Dragicevic
Center of Electric Power and Energy
Technical University of Denmark
Copenhagen, Denmark
tomdr@dtu.dk

***Abstract*—Aiming at the instability problem of traditional power synchronization control (PSC) in a stiff grid, an advanced PSC based on modular multilevel converter (MMC) is proposed in this paper, which can effectively improve converter stability in high short circuit ratio (SCR) scenarios. The key point of the proposed PSC is to eliminate the impact of the arm inductor voltage and capacitor voltage ripple on the converter output voltage, which means a generalized decoupling process in the PSC controller. Based on the decoupling correction, MMC can be treated as a controlled voltage source regardless of the internal impedance circuit and the power oscillation between MMC and the stiff grid can be suppressed effectively. The control strategy is verified and compared with traditional PSC in time simulations.**

Keywords—modular multilevel converter, grid impedance, power synchronization control, short capacity ratio)

I. INTRODUCTION

Modular multilevel converter (MMC) is considered a promising technology for various high-power applications [1]–[3]. Much research has been conducted on it, such as parameter selection [4-5], start-up analysis [6], and current vector control [7-8]. However, with the increasing proportion of new energy in the power system, MMC based on current vector control cannot support the frequency of the power grid, which inevitably decreases the stability of the power grid [9].

The power synchronous control based on the concept of a grid-forming converter which simulates the grid-synchronization approach of traditional generators has become a concerning technology [9], and it can contribute to the frequency support of the grid [11]. The authors of [12] compared PSC and current vector control, and the results showed that the controller instability would occur in PSC when the converter connects to a strong grid, i.e., a system with a large short circuit ratio (SCR).

Pan et al. [13] summarized common grid-synchronization technologies of grid-forming converters, including power synchronous control (PSC) [14], virtual synchronous generator (VSG) [15-16], and power droop control (PDC) [17]. The PSC and PDC have strong robustness under large distributions but do not provide an inertial response, while VSG and PDC with an additional low-pass filter (LPF) can perform frequency inertia but have the risk of instability due to low damping [18]. In reference [14], the transfer function of active power to power angle with PSC was derived in the *DQ* coordinate system, and the existence of the power-frequency resonance phenomenon is pointed out. Literature [19] studied the role of virtual impedance in suppressing power frequency resonance and the impact of inertia constant on the converter stability.

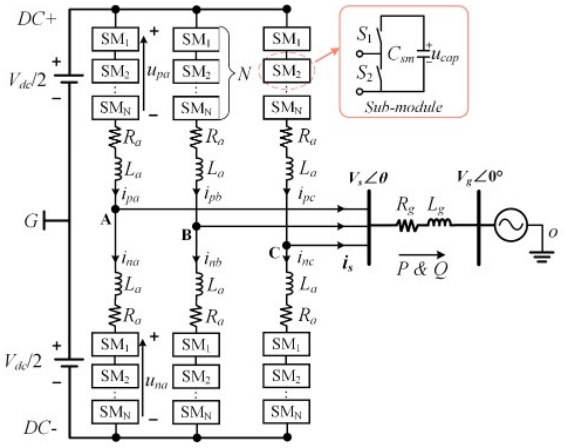

Fig. 1. Topology of MMC connecting to a stiff grid.

However, these studies are based on the topology of two-level converters. Applying this technology directly to MMCS may increase the uncertainty of their controllers because of their complex internal structure, which is more suitable for high-pressure applications. In [20], the LC filter was still used at the output side of MMC which is the same as that of a two-level converter. But usually, no extra LC filter is needed due to the high quality of the output voltage of MMC [23]. Considering the operation of multiple VSG-based MMCs, [21] carried out equivalent integration of multi-MMC based on the power angle relation, which simplified the simulation calculation. However, few pieces of literature analyze the operation control of MMC based on PSC control. This paper carried out theoretical derivation and analysis from this starting point. Since the PSC can work well in a weak grid [12], this paper will focus on the stiff grid scenario with high SCR.

Figure 1 shows the topological structure of MMC. Each arm contains *N* half-bridge sub-modules (SMs). Considering the economy in engineering, the SM capacitance will not very large, so the current flows through SMs will fluctuate the capacitor voltage. It is generally considered that capacitor voltage fluctuation is less than 10% of its average operating voltage at rated power [23]. Inherently, the capacitor voltage fluctuation and dynamic voltage on arm inductors will affect the MMC's actual output voltage. In this paper, the relationship between the PSC output and MMC output is analyzed precisely by considering these factors and the correction method can also be derived to compensate for the loss of reference voltage signal in the MMC internal circuit. In this way, the modified modulation signal is obtained and sent to each SM unit and the dynamic performance of MMC connecting a high-voltage stiff grid can be improved.

The paper is divided as follows. Section II gives the fundamentals of MMC, circulating-current suppression control (CCSC), and the traditional PSC method. Section III dedicates to revealing the precise relationship between the PSC output voltage reference and MMC actual ac-side output voltage. Section III shows the derivation of the proposed correction process of the traditional PSC output. Finally, section IV shows the simulation results of the proposed PSC under different scenarios with varying SCR of the power grid, and a conclusion is given in section V.

II. Fundamental of MMC with PSC

The main circuit of MMC is shown in Fig. 1, in which each phase contains two arms, the upper arm, and the lower arm. Each arm is composed of N submodules (SMs) and an arm inductor L_a. The power loss of each arm is represented by the equivalent resistor R_a. The MMC AC output current is formed by the voltage difference and transmission line inductors between MMC output voltage $V_s\angle\theta$ and stiff grid voltage $V_g\angle 0°$. Subscripts p and n indicate the upper and lower arms respectively. Due to the symmetry of MMC, the three-phase variables differ 120° from each other, so the formula derivation below holds for any phase.

A. Fundamentals of MMC

The phase voltage of the power grid and the MMC ac-side output voltage are defined as follows:

$$\begin{cases} u_g(t) = V_g\cos(\omega_1 t) \\ u_s(t) = V_s\cos(\omega_1 t+\theta) \end{cases} \tag{1}$$

Where V_g and V_s are the phase voltage amplitude of the grid and MMC output and ω_1 denotes the fundamental angular frequency. Note, considering all the variables in this paper are the function of time t, for simplicity, the following formulas will omit the variable t. Hence, based on Kirchhoff's voltage law and current law, the main circuit equation can be directly given here [4]

$$\begin{cases} u_p + R_a i_p + L_a\dfrac{di_p}{dt} + R_g i_s + L_g\dfrac{di_s}{dt} + u_g + u_{oG} = \dfrac{V_{dc}}{2} \\ u_n + R_a i_n + L_a\dfrac{di_n}{dt} - R_g i_s - L_g\dfrac{di_s}{dt} - u_g - u_{oG} = \dfrac{V_{dc}}{2} \end{cases} \tag{2}$$

$$\begin{cases} i_s = i_p - i_n \\ i_{cir} = (i_p + i_n)/2 \end{cases} \tag{3}$$

Where u_p and u_n are the upper and lower arm output voltages, respectively; i_p and i_n are the upper and lower arm currents, respectively; u_{oG} denotes the voltage between the ac-side neutral point (o) and the ground (G). Note, in the balanced system, u_{oG} is quite small concerning line voltage[23], hence it is ignored in this paper; V_{dc} is the dc-side voltage, and the ac-side phase current is denoted as i_s. The phase electromotive force (EMF) (also known as the differential-mode voltage), denoted by u_{diff}, and the phase common-mode voltage, denoted by u_{com} can be obtained by subtracting (2) from (3)

$$\begin{cases} u_{diff} = R_{eq} i_s + L_{eq}\dfrac{di_s}{dt} + u_s \\ u_{com} = -R_a i_{cir} - L_a\dfrac{di_{cir}}{dt} + \dfrac{V_{dc}}{2} \end{cases} \tag{4}$$

Where

$$\begin{cases} u_{diff} = (u_n - u_p)/2 \\ u_{com} = (u_n + u_p)/2 \\ R_{eq} = R_a/2 \\ L_{eq} = L_a/2 \end{cases} \tag{5}$$

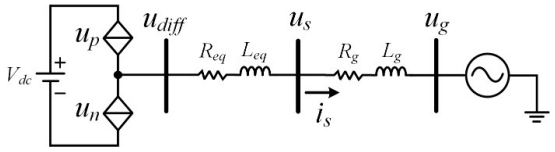

Fig. 2. MMC equivalent circuit.

Based on (4-5), the MMC equivalent circuit can be drawn in Fig. 2, in which, it can be seen that the EMF voltage is the actual AC output voltage of MMC regardless of arm inductors.

From (5), the arm output voltages are controlled by u_{diff} and u_{com}, so the MMC controller needs to generate these two reference voltages u_{diff}^* and u_{com}^*. Since the AC component of circulating current i_{cir} is mainly second-order harmonic [23], which does not contribute to the power transmission and causes power loss, hence the circulating current suppression control (CCSC) has been designed with a PR controller [22] to generate u_{com}^* in (6) and the corresponding controller diagram is also shown in the orange block in Fig. 3. Note, that to eliminate the second-order harmonics in three phases, the common-mode voltage reference u_{com}^* should contain a second-order component [23].

$$\begin{cases} u_{com}^* = \dfrac{V_{dc}}{2} - R_a i_{cir}^* - k_{cir}\left(1+\dfrac{2\alpha_{cir}s}{s^2+(2\omega_1)^2}\right)(i_{cir}^* - i_{cir}) \\ i_{cir}^* = \dfrac{I_{dc}}{3} \end{cases} \tag{6}$$

Where I_{dc} is the DC bus current; k_{cir} and α_{cir} are the P gain and R gain of the PR controller of CCSC and s is the Laplace operator.

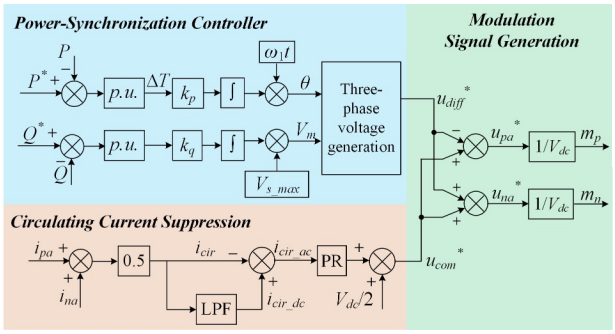

Fig. 3. MMC control diagram containing traditional PSC, CCSC, and Modulation signal generation.

B. Fundamentals of traditional PSC

The power-synchronization mechanism of traditional synchronous machines is the dynamic balance of mechanical torque and electromagnetic torque on the rotor. When the torque on the rotor is unbalanced, the torque difference forces the rotor to accelerate or decelerate to achieve a larger or smaller work angle, thus achieving a new equilibrium, on which PSC control is based [15]. Since the reactance of the

power system is much greater than the resistance, the active power is strongly correlated with the phase angle of the voltage vector, and the reactive power is strongly correlated with the amplitude of the voltage vector, thus the PSC controller ignores the damping torque can be obtained herein (7) and the corresponding controller diagram is also shown in the blue block diagram in Fig. 3.

$$\begin{cases} \theta = \dfrac{k_p}{s}(P^* - P) + \omega_1 t \\ V_m = \dfrac{k_q}{s}(Q^* - Q) + V_{s\_\max} \end{cases} \tag{7}$$

Where k_p and k_q are the gain coefficients in active and reactive power loops; P^* and Q* are the reference value of P and Q; V_{s_max} is the nominal amplitude of the MMC phase voltage; $\omega_1 t$ is the fundamental voltage angle generated by the PSC controller; V_m is the magnitude of PSC output phase voltage and θ is the phase voltage angle. The differential-mode voltage reference u_{diff}^* is generated by θ and V_m.

C. MMC Operation with traditional PSC and CCSC

According to (5) and previous demonstration, the arm output voltage of MMC can be controlled by differential-mode voltage reference u_{diff}^* and common-mode voltage reference u_{com}^*, which are provided by PSC and CCSC. Hence, the arm output voltage reference can be calculated as

$$\begin{aligned} u_p^* &= -u_{diff}^* + u_{com}^* \\ u_n^* &= u_{diff}^* + u_{com}^* \end{aligned} \tag{8}$$

The terms on the left side of (8) can be normalized by dividing the DC voltage V_{dc} [23] and obtaining the upper and lower arm modulation index m_p and m_n. These two modulation indexes are usually limited between 0 and 1 to avoid over-modulation. The additional capacitor voltage balance control is required [4], but it does not influence the analysis results. Hence, in this paper, we assume that the capacitor voltages in the same arm are balanced well. And the obtained modulation index will be applied to each SM and the total arm output voltage can be derived

$$\begin{cases} u_p = N u_{cap\_p} m_p = N u_{cap\_p} \dfrac{-u_{diff}^* + u_{com}^*}{V_{dc}} \\ u_n = N u_{cap\_n} m_p = N u_{cap\_n} \dfrac{u_{diff}^* + u_{com}^*}{V_{dc}} \end{cases} \tag{9}$$

Where the u_{cap_p} and u_{cap_n} are the voltage values of capacitors in the upper and the lower arms. As we get all control signals for the MMC operation, the operation waveform of traditional PSC-controlled MMC connected to a grid with SCR=10 (L_g=31.8 mH) can be obtained by simulation and the results are shown in Fig. 4. The simulation parameters are selected from TABLE I.

Fig. 4 shows that when SCR is 10, the traditional PSC can track the power reference well with a short period transient process. The capacitor voltages contain a DC component, fundamental frequency component, and second-order frequency component while the output currents are mainly composed of fundamental frequency elements [21]. The phase circulating current is almost the DC constant value when the system enters its steady state, which means the CCSC works well and the second harmonic in the circulating current is suppressed effectively. It is noted that the second-harmonic component in the voltage of submodule capacitors can not be mitigated because the capacitor current is the coupling of the grid frequency current and the modulation signal, but this is acceptable and does not affect the stability and economy of the system [23].

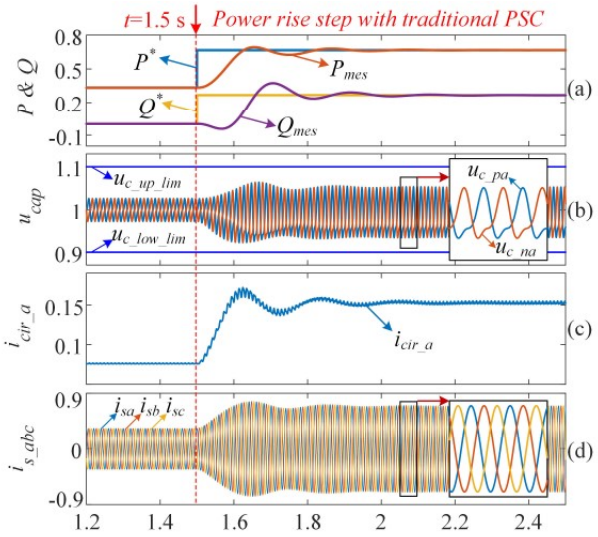

Fig. 4. Simulation waveforms of traditional PSC-controlled MMC with SCR=10. (a) P, Q, and their reference signals, (b) capacitor voltages in phase A, (c) circulating current in phase A, and (d) three-phase output current.

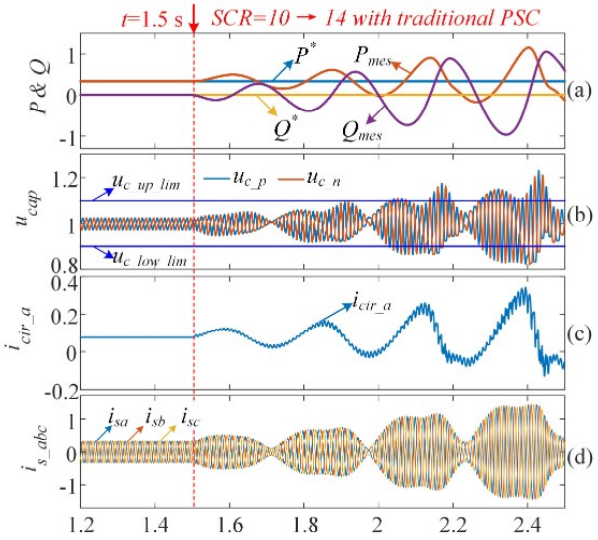

Fig. 5. Simulation waveforms of traditional PSC-controlled MMC when SCR is increased from 10 to 14. (a) P, Q, and their reference signals, (b) capacitor voltages in phase A, (c) circulating current in phase A, and (d) three-phase output current.

III. Oscillation Phenomenon with Traditional PSC and the Derivation of Improved PSC

As the stiff grid generally has higher SCR, MMC needs to adapt to different grid strengths to show its robustness. However, an oscillation phenomenon occurs in the simulation in Fig. 5 when the SCR is increased from 10 to 14. The simulation parameters are selected from TABLE I.

When SCR is 14, the corresponding grid equivalent inductance L_g is 22.74 mH, which is smaller than the MMC

equivalent internal inductance L_{eq} (25.47mH). When the MMC is treated as a voltage source, its internal output impedance will be larger than the impedance of the outer circuit, which means the source is becoming weak.

As mentioned before, there are fluctuations of the capacitor voltage in grid frequency and second-order frequency [23]. It's worth noting that there are also grid frequency and second-order frequency components in the modulation signal. The arm output voltage is determined by both the modulation signal and the capacitor voltage, so there would be differences between the actual differential-mode voltage u_{diff} and the reference voltage u_{diff}^*. In addition, the output voltage u_s is formed after the electromotive force of MMC passes through the equivalent arm inductor, which inevitably causes the actual output voltage of MMC cannot accurately track the output voltage of PSC. In this section, the relationship between u_{diff}^* and u_s will be derived and analyzed.

A. Relationship between traditional PSC output voltage reference and MMC output voltage

According to (3-5) and the modulation process applied to SMs, the MMC output equivalent circuit can be drawn in Fig. 6. The electromotive force voltage is generated by the difference between two arm voltages in the same phase and the arm voltages are controlled by (7). Considering the second-order harmonics in capacitor voltage ripple and the modulation signals, they can be rewritten as

$$\begin{cases} m_p = m_0 - m_{1\omega} + m_{2\omega} \\ m_n = m_0 + m_{1\omega} + m_{2\omega} \\ \dfrac{u_{diff}^*}{V_{dc}} = m_{1\omega} \\ \dfrac{u_{com}^*}{V_{dc}} = m_0 + m_{2\omega} \end{cases} \tag{10}$$

$$\begin{cases} u_{c\_p} = u_{c,0} - u_{c,1\omega} + u_{c,2\omega} \\ u_{c\_n} = u_{c,0} + u_{c,1\omega} + u_{c,2\omega} \end{cases} \tag{11}$$

Where $u_{c,0}$, $u_{c,1\omega}$, and $u_{c,2\omega}$ are the dc, first-order, and second-order components respectively.

Substituting (10-11) to (5), (9) and (4), yield

$$u_{diff} = N\left[(m_0 + m_{2\omega})u_{c,1\omega} + (u_{c,0} + u_{c,2\omega})m_{1\omega}\right] \tag{12}$$

$$\begin{aligned} u_s &= u_{diff} - R_{eq}i_s - sL_{eq}i_s \\ &= \frac{N\left(u_{c,0} + u_{c,2\omega}\right)}{V_{dc}}u_{diff}^* + \frac{Nu_{c,1\omega}}{V_{dc}}u_{com}^* - \left(R_{eq} + sL_{eq}\right)i_s \end{aligned} \tag{13}$$

Equation (13) shows the relationship between PSC output reference voltage u_{diff}^* and real MMC output voltage u_s. It can be seen that the difference between u_{diff}^* and u_s is caused by current flowing through arm inductors and voltage ripples of all SM capacitors inherently. In particular, the even component of the capacitor voltage interacts with the differential mode voltage reference signal u_{diff}^*, while the odd component interacts with the work mode voltage reference signal u_{com}^* to form the actual differential mode voltage u_{diff}.

B. Improved PSC

From (13), it is clear about the real-time relationship of voltage variables in MMC, so we can consider the voltage change in the controller design. Considering the MMC output is well tracking the traditional PSC output, and the corresponding modified modulation signals are m_p^* and m_n^*. Substitute (13) into (9), the modulation index signal can be corrected by the reverse derivation, yield

$$\begin{cases} m_p^* = \dfrac{2\left(-u_{diff}^* + \dfrac{Nu_{c\_mes,n}}{V_{dc}}u_{com}^* - \left(R_{eq} + sL_{eq}\right)i_{s\_mes}\right)}{N(u_{c\_mes,p} + u_{c\_mes,n})} \\ m_n^* = \dfrac{2\left(u_{diff}^* + \dfrac{Nu_{c\_mes,p}}{V_{dc}}u_{com}^* + \left(R_{eq} + sL_{eq}\right)i_{s\_mes}\right)}{N(u_{c\_mes,p} + u_{c\_mes,n})} \end{cases} \tag{14}$$

Where $u_{c\_mes,p,}$ and $u_{c\_mes,n}$ are the measured SM capacitor voltages in the upper arm and the lower arm, respectively; i_{s_mes} is the measurement value of MMC output current. Based on (14), the control block can be drawn in Fig. 6. The purple block in Fig. 6 represents the process from the reference voltage signal to the actual AC output in the MMC circuit. To mitigate the influence of the MMC circuit, the decoupling procedure was designed based on the measured output current and capacitor voltages shown in the blue block in Fig.6. The specific decoupling algorithm is based on the formulas in (14).

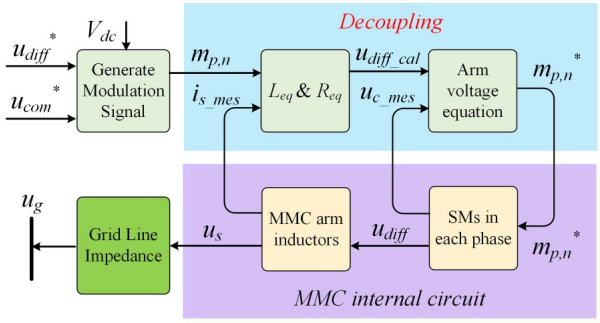

Fig. 6. The control block of the proposed PSC.

From a different perspective, if we can effectively control the MMC output voltage, the electromotive voltage is also directly controlled to some extent. Hence, the arm inductors can be treated as a part of the transmission line inductors. In this way, the increase of total equivalent grid impedance (L_{eq} + L_g) will decline the SCR of the grid, which is more suitable for grid-forming converter operation based on PSC [13].

TABLE I. PARAMETERS OF MMC CIRCUIT AND CONTROLLER

Items	SI	p.u.
Fundamental frequency f	50 Hz	1
Rated capacity S_{rated}	150 MVA	1
Rated line voltage (RMS)	123 kV	1
Power grid SCR	-	14
Grid equivalent inductance L_g	22.74 mH	0.0714
Grid equivalent resistance R_g	0.71 Ω	0.00714
DC-side voltage V_{dc}	220 kV	1.7886
SM capacitance C_{sm}	30.99 μF	1.0271
Arm inductance L_a	50.93 mH	0.16
Arm equivalent resistance R_a	1.6 Ω	0.016
Number of SMs per arm N	100	-
Active power loop gain k_p	-	1
Reactive power loop gain k_q	-	1
P gain of PR controller k_{cir}	50	-
R gain of PR controller α_{cir}	200	-

IV. Simulation

The simulations were carried out in PLECS. The topology of the used MMC is shown in Fig. 1, and the main circuit parameters and control parameters are shown in TABLE I. In TABLE I, "SI" denotes International Unit System; and "p.u." denotes per-unit values.

A. MMC operation with proposed PSC when SCR=14

Figure 5 shows that the traditional PSC cannot maintain the normal operation of MMC when SCR is increased from 10 to 14, which also corresponds to the decrease of system inductance from 31.83 mH to 22.73 mH. To show the improvement of the proposed PSC, at t=3.5 s, the controller is switched from the traditional PSC to the proposed PSC and the transient waveforms are shown in Fig. 7.

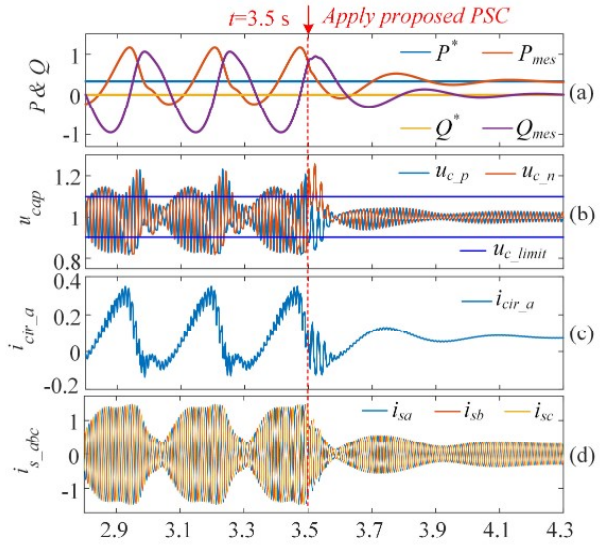

Fig. 7. Simulation waveform of proposed PSC applied at t=3.5s when SCR=14. (a) P, Q, and their reference signals, (b) capacitor voltages in phase A, (c) circulating current in phase A, and (d) three-phase output current.

The transient process in Fig. 7, from 3.5 s to 4.3 s, shows that the MMC output power and internal variables, including capacitor voltages and the circulating current in phase A are becoming stable and maintained within the limitation by applying the proposed PSC. Additionally, we can see that after a short period of the transient process, the capacitor voltages from the upper and lower arms return below the limit after rapid convergence and the double frequency component of the circulation is suppressed accordingly. The system power stabilizes to the reference value after two oscillation cycles. The results show that the proposed PSC is suitable for MMC connecting to a strong power grid with high SCR.

B. Power step response with proposed PSC

To compare the dynamic response characteristic of the proposed PSC to that of the traditional PSC, the power step (the active power is increased from 0.33 p.u. to 0.66 p.u. and the reactive power is increased from 0 to 0.27 p.u is simulated and the results are shown in Fig. 8.

Comparing Fig. 4 and Fig. 8, we can find that during the transient process, the proposed PSC shows a lower oscillation frequency and higher damping and the total transient time is similar, about 0.5 s, which shows that the proposed control strategy improves the stability of MMC in high SCR scenarios without reducing the control performance.

C. The robustness of proposed PSC with higher SCR

As mentioned before, PSC works well in a weak grid with lower SCR, hence, to test the robustness of the proposed PSC, the simulation with higher SCR is also done and the results are shown in Fig. 9.

Before 3.5s, the MMC is operating with P=0.66 p.u. and Q=0.33 p.u. with SCR=14. At t=3.5 s, the SCR is increased to 20, which means L_g is down to 15.9 mH. After 3.5s, the MMC output power shows an oscillation with damping and gradually reaches a steady state. The internal variables show the same dynamic as the output power curves. After a period of the transient process caused by the increase of SCR, the system maintains its stability and enters a new equilibrium point. Therefore, it proves that the proposed PSC shows strong robustness in the face of varying system strength.

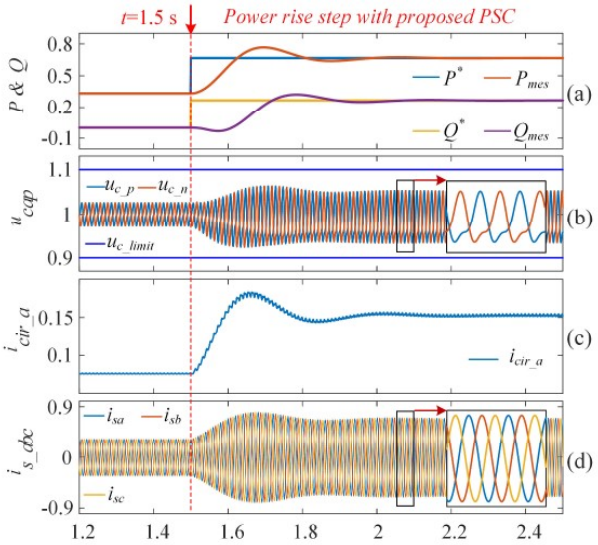

Fig. 8. Power step response with proposed PSC when SCR=14. (a) P, Q, and their reference signals, (b) capacitor voltages in phase A, (c) circulating current in phase A, and (d) three-phase output current.

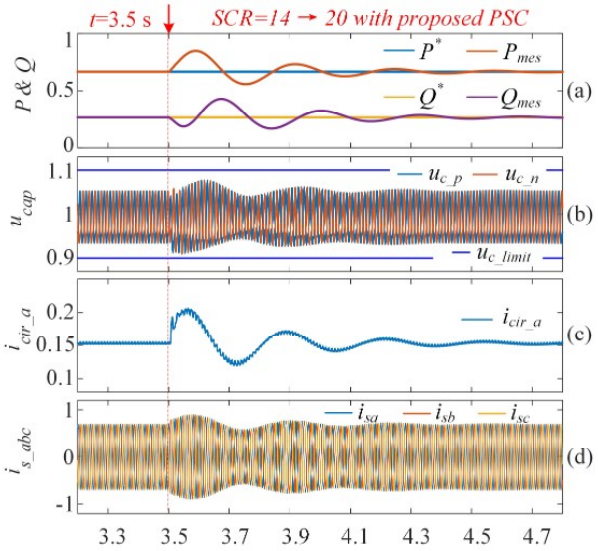

Fig. 9. Transient response with proposed PSC when SCR is increased from 14 to 20. (a) P, Q, and their reference signals, (b) capacitor voltages in phase A, (c) circulating current in phase A, and (d) three-phase output current.

V. Conclusion

In this paper, an investigation of the relationship between voltage reference out of traditional PSC and MMC ac-side output voltage is presented and the unstable phenomenon of MMC operation connecting to the power grid with higher SCR is reproduced with simulation. The obtained results reveal that the voltage of arm inductors and capacitors in each cell does adversely affect the PSC control when the grid impedance is decreased. On this basis, an improved PSC is derived step by step, which can eliminate the dynamic coupling of PSC and the MMC internal caused by the arm inductors and SM capacitors. In simulation results, the proposed PSC exhibits a similar response speed under the power step transient process and can maintain stability with varying SCR of the power system.

References

[1] A. Dekka, B. Wu, R. L. Fuentes, M. Perez, and N. R. Zargari, "Evolution of topologies, modeling, control schemes, and applications of modular multilevel converters," *IEEE Trans. Emerg. Sel. Topics Power Electron.*, vol. 5, no. 4, pp. 1631–1656, Dec. 2017.

[2] M. Priya, P. Ponnambalam, and K. Muralikumar, "Modular multilevel converter topologies and applications—A review," *IET Power Electron*., vol. 12, no. 2, pp. 170–183, Jan. 2019.

[3] D. Ronanki and S. S. Williamson, "Modular multilevel converters for transportation electrification: Challenges and opportunities," *IEEE Trans. Transp. Electrific.,* vol. 4, no. 2, pp. 399–407, Jun. 2018.

[4] Z. Liu, K. -J. Li, J. Wang, W. Liu, Z. Javid, and Z. -d. Wang, "General Model of Modular Multilevel Converter for Analyzing the Steady-State Performance Optimization," *IEEE Trans. on Ind. Electron*., vol. 68, no. 2, pp. 925-937, Feb. 2021.

[5] Y. Li, E. A. Jones, and F. Wang, "Circulating current suppressing control's impact on arm inductance selection for modular multilevel converter," IEEE J. Emerg. Sel. Topics Power Electron., vol. 5, pp. 182-188, 2017.

[6] W. Liu, K. Li, Z. Liu, and M. Wang, "A Simple and Novel Precharging Control Strategy for Modular Multilevel Converter," *IEEE Access*, vol. 7, pp. 170500-170512, 2019.

[7] J. Wang and P. Wang, "Power Decoupling Control for Modular Multilevel Converter," *IEEE Trans. on Power Electron.*, vol. 33, no. 11, pp. 9296-9309, Nov. 2018.

[8] Q. Song, W. Liu, X. Li, H. Rao, S. Xu, and L. Li, "A steady-state analysis method for a modular multilevel converter," IEEE Trans. Power Electron., vol. 28, no. 8, pp. 3702–3713, Aug. 2013.

[9] L. Zhang, L. Harnefors and H. Nee, "Interconnection of Two Very Weak AC Systems by VSC-HVDC Links Using Power-Synchronization Control," *IEEE Trans. on Power Syst*., vol. 26, no. 1, pp. 344-355, Feb. 2011.

[10] J. Fang, H. Li, Y. Tang, and F. Blaabjerg, "On the Inertia of Future More-Electronics Power Systems," *IEEE J. Emerg. Sel. Top. Power Electron*, vol. 7, no. 4, pp. 2130-2146, Dec. 2019.

[11] R. Rosso, X. Wang, M. Liserre, X. Lu and S. Engelken, "Grid-Forming Converters: Control Approaches, Grid-Synchronization, and Future Trends—A Review," *IEEE Open J. Ind. Appl.*, vol. 2, pp. 93-109, 2021.

[12] X. Wang, M. G. Taul, H. Wu, Y. Liao, F. Blaabjerg and L. Harnefors, "Grid-Synchronization Stability of Converter-Based Resources—An Overview," *IEEE Open J. Ind. Appl.*, vol. 1, pp. 115-134, 2020.

[13] D. Pan, X. Wang, F. Liu, and R. Shi, "Transient Stability of Voltage-Source Converters With Grid-Forming Control: A Design-Oriented Study," *IEEE J. Emerg. Sel. Top. Power Electron.*, vol. 8, no. 2, pp. 1019-1033, June 2020.

[14] L. Zhang, L. Harnefors and H. Nee, "Power-Synchronization Control of Grid-Connected Voltage-Source Converters," *IEEE Trans. on Power Syst*., vol. 25, no. 2, pp. 809-820, May 2010.

[15] H.-P. Beck and R. Hesse, "Virtual synchronous machine," in *Proc. 9th Int. Conf. Elect. Power Qual. Utilisation*, Barcelona, Spain, Oct. 2007, pp. 1–6.

[16] Q.-C. Zhong, P.-L. Nguyen, Z. Ma, and W. Sheng, "Self-synchronized synchronverters: Inverters without a dedicated synchronization unit," *IEEE Trans. Power Electron*., vol. 29, no. 2, pp. 617–630, Feb. 2014.

[17] S. D'Arco and J. A. Suul, "Equivalence of virtual synchronous machines and frequency-droops for converter-based microgrids," IEEE Trans. Smart Grid, vol. 5, no. 1, pp. 394–395, Jan. 2014.

[18] J. Liu, Y. Miura, and T. Ise, "Comparison of dynamic characteristics between virtual synchronous generator and droop control in inverterbased distributed generators," IEEE Trans. Power Electron., vol. 31, no. 5, pp. 3600–3611, May 2016.

[19] Y. Hu, Y. Shao, R. Yang, X. Long, and G. Chen, "A Configurable Virtual Impedance Method for Grid-Connected Virtual Synchronous Generator to Improve the Quality of Output Current," *IEEE J. Emerg. Sel. Top. Power Electron*, vol. 8, no. 3, pp. 2404-2419, Sept. 2020.

[20] B. Peng, X. Yin, J. Shen, and J. Wang, "Application of virtual synchronization control strategy in MMC based VSC-HVDC system," *2014 Asia-Pacific Pow. Energy Eng. Conf.,* (APPEEC), 2014, pp. 1-6.

[21] C. Li, J. Xu, and C. Zhao, "A Coherency-Based Equivalence Method for MMC Inverters Using Virtual Synchronous Generator Control," in *IEEE Trans. on Power Deliv*., vol. 31, no. 3, pp. 1369-1378, June 2016.

[22] K. Sharifabadi, L. Harnefors, H. P. Nee, et al. "Design, control, and application of modular multilevel converters for HVDC transmission systems," *John Wiley & Sons*, 2016.

[23] Z. Liu, K. Li, J. Wang, Z. Javid, M. Wang, and K. Sun, "Research on Capacitance Selection for Modular Multi-Level Converter," in IEEE Trans. on Power Electron., vol. 34, no. 9, pp. 8417-8434, Sept. 2019.